Biomaterials 185 (2018) 310–321

Contents lists available at ScienceDirect

Biomaterials

journal homepage: www.elsevier.com/locate/biomaterials

Rapid 3D bioprinting of decellularized extracellular matrix with regionally varied mechanical properties and biomimetic microarchitecture

Xuanyi Ma[a,1], Claire Yu[b,1], Pengrui Wang[c], Weizhe Xu[a], Xueyi Wan[d], Cheuk Sun Edwin Lai[e], Justin Liu[c], Anna Koroleva-Maharajh[b], Shaochen Chen[a,b,c,e,*]

[a] Department of Bioengineering, University of California, San Diego, La Jolla, CA, 92093, USA
[b] Department of NanoEngineering, University of California, San Diego, La Jolla, CA, 92093, USA
[c] Materials Science and Engineering Program, University of California, San Diego, La Jolla, CA, 92093, USA
[d] Division of Biological Sciences, University of California, San Diego, La Jolla, CA, 92093, USA
[e] Chemical Engineering Program, University of California, San Diego, La Jolla, CA, 92093, USA

ARTICLE INFO

Keywords:
3D bioprinting
Decellularized extracellular matrix
Cancer invasion
Liver fibrosis
Tissue engineering

ABSTRACT

Hepatocellular carcinoma (HCC), as the fifth most common malignant cancer, develops and progresses mostly in a cirrhotic liver where stiff nodules are separated by fibrous bands. Scaffolds that can provide a 3D cirrhotic mechanical environment with complex native composition and biomimetic architecture are necessary for the development of better predictive tissue models. Here, we developed photocrosslinkable liver decellularized extracellular matrix (dECM) and a rapid light-based 3D bioprinting process to pattern liver dECM with tailorable mechanical properties to serve as a platform for HCC progression study. 3D bioprinted liver dECM scaffolds were able to stably recapitulate the clinically relevant mechanical properties of cirrhotic liver tissue. When encapsulated in dECM scaffolds with cirrhotic stiffness, HepG2 cells demonstrated reduced growth along with an upregulation of invasion markers compared to healthy controls. Moreover, an engineered cancer tissue platform possessing tissue-scale organization and distinct regional stiffness enabled the visualization of HepG2 stromal invasion from the nodule with cirrhotic stiffness. This work demonstrates a significant advancement in rapid 3D patterning of complex ECM biomaterials with biomimetic architecture and tunable mechanical properties for *in vitro* disease modeling.

1. Introduction

Hepatocellular carcinoma (HCC) is ranked as the fifth most common malignant cancer and the second most frequent cause of cancer related mortality worldwide [1]. Over 80% of HCCs develop and progress in the form of advanced liver fibrosis or cirrhosis, which is characterized by the development of stiff hepatocellular nodules surrounded by fibrous bands [2,3]. HCC development and progression are strongly affected by the liver extracellular matrix (ECM) stiffness and correlated to stiffness values greater than that of healthy liver parenchyma [4,5]. In addition, the progression of HCC also involves invasion of tumor tissue into the fibrous septa [6]. Traditional approaches to study HCC progression involved simply regulating 2D substrate stiffness, which, however, is not representative of the 3D mechanical environment in native liver and therefore could incur results inconsistent with those from 3D approaches [7–11]. Current studies examining the liver mechanical properties with 3D matrix models, however, do not reflect the clinically reported stiffness range and the microarchitecture of cirrhotic liver and thus provide less insightful results in understanding HCC progression under diseased conditions [9,12]. In addition to the importance of a relevant 3D mechanical environment, the biomaterial used to study cancer progression has also been shown to play an important role in regulating cancer growth and proliferation [13]. Current hydrogel matrices used to modulate stiffness, including alginate and gelatin [9,12], lack the biochemical cues inherent in the native liver ECM. Therefore, a biomimetic platform combining liver ECM as a tissue-specific biomaterial and a 3D mechanical environment with tissue-scale organization relevant to diseased liver is critical in studying the biomechanical contributions of the cirrhotic environment on HCC growth and invasion.

Native liver ECM is composed of a wide range of proteins, collagens, glycosaminoglycans, and growth factors that could provide a complex

* Corresponding author.Department of NanoEngineering, University of California San Diego, 9500 Gilman Drive Mail code, 0448, La Jolla, CA, 92093-0448, USA.
E-mail address: chen168@eng.ucsd.edu (S. Chen).
[1] These authors contributed equally to this publication.

https://doi.org/10.1016/j.biomaterials.2018.09.026
Received 7 July 2018; Received in revised form 22 August 2018; Accepted 16 September 2018
Available online 18 September 2018
0142-9612/

microenvironment to better support liver cell viability and functionality compared to simple protein matrices used in current 2D or 3D cell culture systems [14–16]. More importantly, it has been widely established that liver decellularized extracellular matrix (dECM) supports liver progenitor differentiation as well as hepatocyte and HCC cell line culture, and is regarded as a promising naturally-derived biomaterial for *in vitro* liver cell culture [17–19]. To date, the use of liver dECM in *in vitro* cell culture is largely limited to 2D coatings or 3D gels in simple geometries [19–21], which lack a biomimetic design that mimics HCC nodule surrounded by fibrous bands. In addition, the lack of methods tuning the mechanical property of dECM materials restrain their application to pathological conditions where tissue architecture and mechanical properties are both important in affecting disease progression. Digital light processing (DLP)-based 3D bioprinting, with the capability to pattern a wide range of functional elements including live cells, biomolecules, and nanoparticles provides superior speed for the fabrication of complex 3D geometries and precise control over material properties [22–24]. Here we present a DLP-based rapid 3D bioprinting approach to fabricate cellularized liver dECM-based scaffolds with tunable mechanical properties to serve as a platform for studying the effects of pathologically relevant 3D matrix stiffness on HCC progression and invasion. Furthermore, we demonstrated a novel proof-of-concept cancer tissue platform with a biomimetic fibrous septa design to visualize HepG2 cell invasive behavior that was consistent with our findings at the genetic level.

To the best of our knowledge, this is the first report for DLP-based 3D bioprinting of liver dECM-based hydrogels with tunable mechanical properties for HCC growth and invasion study in a pathological mechanical environment. This *in vitro* dECM-based 3D biomimetic liver platform can be used to study the behavior of various liver cancer cells under specific fibrotic environments to help elucidate disease mechanisms in biological studies and for applications in preclinical drug screening.

2. Materials and methods

2.1. Liver decellularization

Fresh porcine liver was sourced from three month old healthy Yorkshire pigs (40–45 kg) supplied by S&S Farms (Ramona, CA), which is an approved vendor by the Institutional Animal Care and Use Committee (IACUC) at the University of California San Diego (UCSD). The pigs were euthanized with an overdose of pentobarbital and the fresh liver tissues were immediately harvested and transported on ice to the lab. Excess blood was rinsed and tissues were stored in D-PBS supplemented with 1% (vol/vol) antibiotic/antimycotic (ABAM) (ThermoFisher Scientific) at −80 °C prior to decellularization. All steps from tissue procurement to storage was performed within 2–3 h of harvesting to ensure preservation of tissue integrity and quality. For all experiments, at least three entire livers were pooled and processed into liver dECM to minimize potential batch-to-batch variations.

To prepare the liver decellularized extracellular matrix (dECM), all steps were performed in an incubator shaker set at 37 °C and 120 rpm and all solutions were supplemented with 1% (vol/vol) ABAM and 0.01 mM phenylmethylsulfonyl fluoride (PMSF) (Sigma Aldrich). Frozen liver tissues were thawed and minced finely with scissors into 0.5 cm^3 pieces. The minced liver was then subjected to three cycles of freeze thaw with 2 h washes in hypotonic solution in between. The tissues were then rinsed three times with 1X D-PBS for 30 min each and washed in 1% (wt/vol) sodium dodecyl sulfate (SDS) (Sigma Aldrich) in D-PBS for 48 h with 2–3 solution changes per day until white in appearance. The resulting tissue was rinsed thoroughly in deionized water for an additional 24 h with 2–3 solution changes per day and stored in 70% (vol/vol) ethanol at 4 °C until further use.

2.2. Histological and immunohistochemical (IHC) staining of liver dECM

To visualize residual cellular material and microarchitecture, liver dECM and native liver controls were prepared by fixing in 4% (wt/vol) paraformaldehyde (PFA) buffer solution (Wako) overnight at 4 °C followed by rinsing three times in 1X D-PBS and immersing in 70% (vol/vol) ethanol. The tissues were then paraffin embedded, sectioned at 5 μm thickness, and stained with hematoxylin and eosin (H&E). Images were taken using a Keyence BZ-9000 microscope with multicolor CCD camera.

IHC staining was used to visualize the presence of key ECM components post liver decellularization. Unfixed liver dECM samples were prepared by immersing in 30% (wt/vol) sucrose solution overnight and cryoembedded in Tissue-Tek® O.C.T compound (VWR). Samples were then cryosectioned at 10 μm thickness and incubated for 1 h at room temperature in blocking solution prepared from 10% (vol/vol) goat serum (Vector Laboratories) in 1X D-PBS with 0.2% (vol/vol) Tween 20 (Spectrum Chemicals). Next, the sections were stained with the following primary antibodies diluted in blocking solution: monoclonal mouse anti-collagen I (1:2000, Abcam), polyclonal rabbit anti-collagen IV (1:100, Abcam), monoclonal mouse anti-fibronectin (1:100, Abcam), and polyclonal rabbit anti-laminin (1:100, Abcam). Collagen I antibody was incubated at room temperature for 1 h while collagen IV antibody was incubated for 1 h at 37 °C. Fibronectin and laminin antibodies were incubated at 4 °C overnight. Afterwards, the sections were rinsed three times with 1X D-PBS and incubated for 1 h at room temperature with the following secondary antibodies both diluted in blocking solution: CF647 donkey anti-rabbit IgG (H + L) (1:200, Biotium) and CF647 donkey anti-mouse IgG (H + L) (1:200, Biotium). The sections were rinsed again three times with 1X D-PBS and mounted with Fluoroshield Mounting Medium (Abcam). No primary controls were included on each slide and native tissue controls were used to verify the specificity of each antibody. Fluorescent images were taken using a Leica DMI 6000-B microscope.

2.3. Scanning electron microscopy (SEM) of liver dECM ultrastructure

For qualitative assessment of the preserved liver dECM ultrastructure, samples were prepared by gradual dehydration in ethanol followed by chemical drying in hexamethyldisilazane (Sigma Aldrich) overnight. The dried samples were then sputtered with iridium for 7 s and imaged using a Zeiss Sigma 500 scanning electron microscope.

2.4. Quantification of dsDNA, GAG, and collagen content

To prepare the samples for dsDNA and glycosaminoglycan (GAG) quantification, 50 mg of lyophilized liver dECM or native liver control was measured and placed into a 1.5 mL eppendorf tube. Then 1 mL of papain digest solution composed of 0.1 mg/mL papain (Sigma-Aldrich) in 0.2 M sodium phosphate buffer solution (pH 6.4) was added to each sample. The samples were then digested at 65 °C for 20 h with periodic vortexing, followed by centrifugation at 10,000 rpm for 10 min. The supernatant was collected and used to measure the residual dsDNA content with the Quant-iT™ PicoGreen dsDNA (ThermoFisher Scientific) and the GAG content with the Blyscan™ Glycosaminoglycan Kit (Biocolor), respectively, according to the manufacturer's protocols.

To quantifying the residual collagen content, 10 mg of lyophilized liver dECM or native liver control was measured and placed into a 1.5 mL polypropylene tube. Next, 100 μL of deionized water was added and vortexed on high for 30 s to homogenize the sample followed by the addition of 100 μL of 12 M HCl (MilliporeSigma). The samples were vortexed briefly and hydrolyzed for 3 h at 120 °C followed by centrifugation at 10,000 rpm for 10 min. The supernatant was collected and used to quantify the collagen content using the Hydroxyproline Assay Kit (Sigma-Aldrich) according the manufacturer's methods.

2.5. Preparation of liver dECM and collagen I solutions

To prepare the liver dECM solution, the liver dECM was decontaminated by washing in 70% (vol/vol) ethanol for 24 h in an incubator shaker. Sterile deionized water was then used to rinse the tissue of residual ethanol for another 24 h prior to freezing and lyophilization for 48 h. Using a Restch™ MM400 mixer mill, the lyophilized liver dECM or collagen I (Sigma-Aldrich) was loaded into the milling chamber containing two 10 mm stainless steel milling balls, immersed in liquid nitrogen for 3 min, and cryomilled for 2 min. Following this, the liver dECM or collagen I powder (10 mg/mL, Sigma-Aldrich) was solubilized using pepsin (Sigma-Aldrich) at 1 mg/mL in 0.1 M HCl for 24 h at room temperature on a bench-top shaker. The solution was then neutralized with NaOH then frozen and lyophilized overnight. Next, the lyophilized solutions were cryomilled again by immersing in liquid nitrogen for 3 min and cryomilled for 2 min to yield a fine powder that can be readily reconstituted.

2.6. Material synthesis and prepolymer solution preparation

GelMA was synthesized according to the procedures reported in previous publications [22,23]. In brief, porcine skin gelatin type A (Sigma Aldrich) was mixed at 10% (wt/vol) in D-PBS without calcium and magnesium (Life Technologies) and stirred at a temperature of 60 °C. After gelatin was fully dissolved, methacrylic anhydride (MA) (Sigma Aldrich) was added to the gelatin solution to reach a concentration of 8% (vol/vol). The mixture was then stirred for 3 h at a temperature of 60 °C, followed by a dilution with warm D-PBS. To remove the unreacted MA groups from the solution, it was then dialyzed against distilled water using dialysis tubing (13.5-kDa cutoff; Spectrum Laboratories) for a week at 45 °C. Following dialysis, GelMA solution was frozen overnight at −80 °C and lyophilized in a freeze dryer (Labconco) until further use.

Lithium phenyl-2,4,6 trimethylbenzoylphosphinate (LAP) was used as a photoinitiator for our light-based bioprinting process. It was synthesized according to previous publications [22,23]. Dimethyl phenylphosphonite (3.0 g; Sigma Aldrich) was continuously stirred while an equimolar amount of 2,4,6-trimethylbenzoyl chloride (3.2 g, Acros Organics) was added dropwise. The reaction mixture was stirred for 18 h under argon at room temperature, and then it was heated to 50 °C. A four-fold excess of lithium bromide (6.1 g; Sigma Aldrich) in 100 mL of 2-butanone (Sigma-Aldrich) was added to the mixture. The reaction was continued with constant stirring for another 10 min while a white solid was precipitated. The mixture was cooled to room temperature, and maintained at the temperature for 4 h. The precipitates were filtered and washed 3 times with 2-butanone to remove unreacted lithium bromide. The product was dried by vacuum.

To prepare a stock of prepolymer solution, freeze-dried GelMA foam was weighed and dissolved into 1.8% (wt/vol) LAP solution in D-PBS to form a 15% (wt/vol) GelMA prepolymer stock solution. The stock solution was sterilized by syringe filters (Millipore), aliquoted, and stored at 4 °C in the dark. Before bioprinting, the stock prepolymer solution was diluted with D-PBS to form 10% (wt/vol) GelMA prepolymer solution with 1.2% (wt/vol) LAP. Next, the cryomilled liver dECM or collagen I powder was reconstituted to with 1X D-PBS to 100 mg/mL stock solution. The GelMA and liver dECM or collagen I stock solutions were then mixed in a 1:1 ratio by volume to yield a final solution concentration of 5% (wt/vol) GelMA + 5% (wt/vol) liver dECM or collagen I + 0.6% (wt/vol) LAP for subsequent printing.

2.7. HepG2 maintenance and cell suspension preparation

HepG2 cell line was purchased from ATCC and maintained in DMEM (Thermo Fisher Scientific) with 10% (vol/vol) fetal bovine serum (FBS) (Gibco). Cells were passaged every four days upon 80–90% confluence using 0.25% (vol/vol) Trypsin-EDTA (Thermo Fisher Scientific). Prior to bioprinting, cells were dissociated using 0.25% (vol/vol) Trypsin-EDTA and counted with a hemacytometer. A cell suspension in growth medium at 2.5 million cells per mL was prepared and 50 μL was aliquoted into each 1.5 mL centrifuge tube. Immediately before printing, cell aliquots were pelleted by centrifugation at 200 rpm for 3 min and the supernatant was carefully removed. The cell aliquots were placed on ice and used within 2 h. Immediately prior to printing, 50 μL of pre-warmed prepolymer solution was added to each cell aliquot and gently mixed prior to loading into the printing chamber.

2.8. Bioprinting of acellular and cell embedded hexagonal constructs

Rapid 3D bioprinting of hexagonal constructs with and without cells was carried out using a digital micromirror device (DMD)-based system. This custom built printing platform consists of a LED light source at 365 nm (Hamamatsu), a DMD chip (DLP Technology of Texas Instruments), aligning optics, and a movable stage controlled by a motion controller (Newport). The digital pattern of the hexagon was designed in Adobe Photoshop and loaded to the DMD chip before bioprinting.

For printing an acellular construct, the 5% (wt/vol) GelMA – 5% (wt/vol) dECM prepolymer solution was loaded to the space between a methacrylated coverslip fixed on the motion controller stage and a fixed polydimethylsiloxane (PDMS) layer, and then polymerized into a hexagonal construct following light exposure. For printing a construct with cells encapsulated, the 5% (wt/vol) GelMA – 5% (wt/vol) dECM prepolymer solution was added to the cell pellet to resuspend the cells in prepolymer solution. This cell-material mixture was then loaded to the same space between a methacrylated coverslip fixed on the motion controller stage and a fixed PDMS layer, and then polymerized into a hexagonal construct following light exposure. The height of the construct was controlled by the motion controller and set to be around 200 μm. Bioprinted constructs were then rinsed once in D-PBS solution, followed by another rinse in medium and incubation in medium at 37 °C and 5% CO_2. Medium was replaced the next day following bioprinting and then every other day.

2.9. Mechanical property measurements

Bioprinted acellular and cell embedded constructs were tested for their mechanical properties at 24 h, 72 h, and 7 day time points. The samples were incubated at 37 °C and 5% CO_2 following bioprinting until the measurement time points. Mechanical property measurements of the samples were carried out using a commercially available MicroSquisher (CellScale). Before recording measurements, each sample was preconditioned by compressing at 4 μm/s to remove hysteresis caused by internal friction. The compression test was conducted at 10% strain with a 2 μm/s strain rate. The elastic modulus was then calculated using an in-house MATLAB code with the force and displacement data collected from the SquisherJoy software.

2.10. Molecular diffusion assessment

TRITC-dextran of molecular weight 4.4 kDa and 60–85 kDa (Sigma) were resuspended in D-PBS at a concentration of 0.5 mg/mL 3D printed liver dECM-based scaffolds were incubated in TRITC-dextran solutions at 37 °C for 0, 1, 10, 30 and 60 min then rinsed and imaged using a fluorescence microscope. Intensity profiles of samples were generated using ImageJ and plotted using MATLAB. Average intensity from each intensity profile was computed and compared across conditions.

2.11. Viability evaluation and analysis

Viability evaluation of HepG2 cells encapsulated in scaffolds of various stiffness was performed using commercially available Live/Dead™ Viability/Cytotoxicity kit (Life Technologies) based on calcein

AM and ethidium homodimer-1 (EthD-1). Staining was carried out at 24 h, 72 h, and 7 day time points following bioprinting. Samples were washed once with D-PBS following culture medium removal and then incubated with 2 μM calcein AM and 4 μM EthD-1 solution at 37 °C for 15 min. Imaging acquisition by a Leica DMI 6000B microscope (Leica Microsystems) using a 5× objective was immediately carried out following incubation. ImageJ (National Institutes of Health) was used to view and merge channels. For the quantification of live cell percentage in cell suspension used immediately before the bioprinting process, HepG2 cells were enzymatically detached from culture flask, centrifuged and resuspended in culture medium, aliquoted into 1.5 mL centrifuge tubes and stored on ice for 30–60 min. Then cell suspension was mixed with trypan blue and live and dead cells were counted using hemocytometer.

2.12. Immunofluorescence staining and imaging of printed cell-embedded scaffolds

Samples were fixed in 4% (wt/vol) PFA solution (Wako) for 15 min at room temperature. Before imaging, fixed samples were blocked and permeabilized using 2% (wt/vol) bovine serum albumin (BSA) (Gemini Bio-Products) solution with 0.1% (vol/vol) Triton X-100 (Promega) for 1 h at room temperature. For human albumin and E-cadherin staining, samples were incubated with mouse monoclonal antibodies against human E-cadherin (1:100; Abcam) and rabbit monoclonal antibodies against human albumin (1:100; Abcam) overnight at 4 °C. Following primary antibody incubation, samples were washed three times with D-PBS at room temperature. Secondary antibody incubation was carried out using fluorophore-conjugated anti-IgG antibodies (1:200, Biotium) in 2% (wt/wt) BSA (Gemini Bio-Products) solution for 1 h at room temperature. Hoechst 33342 (1:2000; Life Technologies) nucleus counterstain was also performed simultaneously with the secondary antibody incubation. Fluorescently stained samples were stored in D-PBS with 0.05% (wt/vol) sodium azide (Alfa Aesar) at 4 °C after washing three times with D-PBS. Samples were imaged within one week of staining.

2.13. RNA isolation and reverse transcription-polymerase chain reaction (RT-PCR)

HepG2 cells cultured as 2D monolayer in flasks were firstly pelleted then treated with ice cold TRIzol reagent (Ambion, Life Technologies) for 5 min and stored in −80 °C freezer before RNA extraction. Bioprinted samples were firstly broken down to smaller pieces using pipette tips to expose embedded cells. The broken samples were then treated with ice cold TRIzol and pipetted for 5 min before storage in −80 °C fridge. Total RNA from each TRIzol sample was isolated using Direct-zol RNA MiniPrep Kit (Zymo Research) according to the manufacturer's instruction. Extracted RNA samples were stored in −80 °C freezer before RT-PCR experiments.

Reverse transcription was carried out to synthesize cDNA using PhotoScript® first strand cDNA synthesis kit (New England BioLabs) according to manufacturer's instruction. Real-time RT-PCR was performed using KAPA SYBR Fast qPCR kit (KAPA Biosystems) with specific primers (Integrated DNA Technologies) and detected by StepOne™ Real-Time PCR System (ThermoFisher). Relative quantification was carried out based on the threshold cycle (Ct) of each sample and the values were normalized against the housekeeping gene, glyceraldehyde 3-phosphate dehydrogenase (GAPDH).

2.14. Bioprinting of a liver cancer tissue platform for invasion study

Rapid 3D bioprinting of a liver cancer tissue platform was carried out using the same DMD-based bioprinting platform as described in the above section. Three hexagons of HepG2 cells, each consisting of cells tracked with a specific fluorescence color to distinguish the matrix stiffness were printed. These steps were followed by a final print of the fibrous septa in between the hexagons. Prior to printing, three digital patterns of the hexagon and one pattern of fibrous septa were designed in Adobe Photoshop and loaded into the DMD chip. One day before printing, three flasks of HepG2 cells were tracked using CellTracker™ green CMFDA dye (5 μM, 1 h incubation), CellTracker™ orange CMTMR dye (5 μM, 1 h incubation), and Qtracker™ 705 cell labeling kit (15 nM, overnight incubation) respectively to label live cells with a specific color. Cells tracked by Qtracker™ 705 dye (imaged as in red pseudo color) were encapsulated in the soft matrix, cells tracked by green CMFDA dye (imaged as in green pseudo color) were encapsulated in the matrix of medium stiffness, cells tracked with orange CMTMR dye (imaged as in yellow pseudo color) were encapsulated in the stiff matrix representative of cirrhotic liver modulus.

On the day of printing, HepG2 cells of each color were digested and aliquoted as described in the previous section for cell suspension preparation. The 5% (wt/vol) GelMA – 5% (wt/vol) dECM prepolymer solution was added to the cell pellet to resuspend the cells in prepolymer solution. Next, 20 μL of the cell-material mixture with one tracking color was pipetted into the space between a methacrylated coverslip fixed on the motion controller stage and a fixed PDMS layer and then polymerized into a hexagonal construct following light exposure. The printed construct was rinsed with sterile D-PBS, aspirated dry, and the next cell-material mixture was loaded to the same space to print. The rinsing and printing was repeated one more time to print the third cell embedded hexagon. Following the printing of cells tracked with all three colors, 5% (wt/vol) GelMA – 5% (wt/vol) collagen I prepolymer solution was added to the stage and the fibrous septa-like structure was printed in between the hexagons. The height of the entire construct was controlled by the motion controller and set to be around 200 μm. The bioprinted constructs were then rinsed once in D-PBS, followed by another rinse in medium and incubation in medium at 37 °C and 5% CO_2. Medium was replaced the next day following bioprinting and then every other day.

2.15. Image acquisition and processing

Brightfield and fluorescence images of the bioprinted samples were acquired with a Leica DMI 6000B microscope (Leica Microsystems) using a 5× objectives. Confocal immunofluorescence images were acquired with a 40X, 0.8N.A. water-immersion objective attached to an Olympus FV1000 microscope (Olympus America, Inc.). ImageJ (National Institutes of Health) was used to merge channels, perform z-projection, render 3D reconstruction, and carry out measurements for confocal images and stacks.

2.16. Quantification of viability and spheroid size

Cell viability was analyzed by using ImageJ based on the images taken by Leica DMI 6000B microscope. Fluorescent channels showing live (green) and dead (red) cells were merged. Live cells and dead cells were counted and the percent of live cells were calculated based on the counts. The spheroid size was quantified using previously described approach [22]. In brief, ImageJ was used to generate a z-projection image from the z-stacks of HepG2 cell spheroids within the bioprinted model. The diameters of the spheroids in the z-projection image were measured in the direction of 0, 45, 90, and 135° by ImageJ and averaged for comparison. Three individual samples were used for each condition.

2.17. Quantification of HepG2 cell outgrowth

Fluorescence images of HepG2 cells tracked in each color (representing each matrix stiffness) on day 1, 3 and 7 were taken by Leica microscope as described in the above section. During the analysis of each sample, a hexagonal outline was drawn using the polygon

selection tool in ImageJ on the bright field image to select out one hexagon. This hexagonal outline was then restored in the corresponding fluorescence channel and used to clear out all fluorescence signals within the hexagon. The total area of the outgrown cells in this tracked color was then measured using the particle analysis tool in ImageJ. These steps were repeated for each fluorescence channel to quantify the total outgrowth area of cells from each of the three hexagons. Five individual samples were used for each condition per time point.

2.18. Statistical analysis

Sample populations were compared using two-tailed Student's t-test when there were two conditions for comparison. In the case of comparing three conditions together, sample populations were compared using one-way ANOVA. P value smaller than 0.05 was used as the threshold for statistical significance. Data points on the graphs represent mean values with error bars representing standard error of the mean. All statistical analysis was done using GraphPad Prism version 6.0 (GraphPad Software).

3. Results

3.1. Rapid 3D bioprinting of liver dECM hydrogel with key liver ECM components

To develop photocrosslinkable liver dECM-based hydrogel materials for DLP-based rapid 3D bioprinting, liver dECM was combined with photocrosslinkable gelatin methacrylate (GelMA) to produce a printable solution. The liver decellularization process involved sequential steps of detergent-based washing, pepsin solubilization, freeze drying, and cryomilling to produce a fine liver dECM powder that can be reconstituted upon use (Fig. 1A i-vi). The process to remove cellular content was optimized to preserve the ultrastructure of the native ECM as well as collagen fibrils and key ECM constituents (Fig. 1B). The absence of nuclear staining in the H&E stained sections showed the successful removal of cells. Additional DNA quantification of the liver dECM demonstrated a negligible amount of residual DNA of less than 50 ng/mg dry weight [25], which further confirms the successful removal of cellular content (Figure S1A, Supporting Information). Following this, the preservation of major ECM constituents was assessed for the liver dECM. The optimized decellularization process was able to retain approximately 30% of GAG content in the liver dECM compared to that of native liver (Figure S1B, Supporting Information). Moreover, after decellularization the collagen content was enriched in the liver dECM relative to the native liver control (Figure S1C, Supporting Information). The liver dECM solution was then mixed with GelMA prepolymer to form a photocrosslinkable hydrogel solution for rapid 3D bioprinting. Here, our DLP-based 3D bioprinter that uses a digital micromirror device (DMD) chip to generate layered, digital optical patterns for photopolymerization was used to fabricate liver dECM-based scaffolds with user defined design (Fig. 1C). More specifically, a hexagonal digital pattern with dimensions adjusted to approximate the size of one liver lobule (1 mm diameter) was used for printing the dECM-based scaffolds (Fig. 1D). The printed constructs were stained and visualized for the presence of key ECM components. Overall, the dECM-GelMA hydrogels showed positive staining of collagen I, collagen IV, fibronectin, and laminin similar to those observed in the liver dECM stains (Fig. 1E).

Together, we showed successful removal of cellular content while preserving key liver ECM components in the liver dECM hydrogel. Combining liver dECM with GelMA produced a photocrosslinkable solution that can be readily printed into hexagonal lobule shapes using DLP-based rapid 3D bioprinting.

3.2. Photocrosslinked liver dECM-based scaffold supports HCC culture in vitro

Upon successful liver decellularization to produce a photocrosslinkable dECM-based hydrogel, *in vitro* culture studies using HepG2 cells, a widely used HCC line, were performed to examine the cell viability and liver-specific gene expression of encapsulated cells. Here, we compared the culture of HepG2 cells using liver dECM-based scaffolds to collagen I-based scaffolds and GelMA scaffolds, which have been commonly used in *in vitro* liver cell culture and for creating tissue engineered liver constructs [22,26]. To eliminate possible effects contributed by the scaffold mechanical properties on HepG2 cell viability and expression profile, the stiffness of all three scaffolds were kept within the healthy liver range (Figure S2, Supporting Information). Viability studies demonstrated by Live/Dead™ staining of the HepG2 cells over 7 days showed a similar level of viability in the liver dECM and collagen I-based scaffolds, however, a lower number of live cells were observed in the GelMA scaffolds at the 3-day and 7-day time points (Fig. 2A). Fluorescence images of HepG2 cells cultured in each of the three groups all showed positive staining for both albumin (ALB) and E-cadherin (ECAD), suggesting that all three types of scaffolds supported albumin production and epithelial cell junction formation (Fig. 2B). Furthermore, a significantly lower expression of the proliferation marker gene *MKI67* in cells cultured in GelMA was observed when compared to the liver dECM-based and collagen I-based scaffolds at 7 days (Fig. 2C), which is consistent with the observed lower viability stains in the GelMA samples at 7 days. There was also a trend for higher expression of the metabolic markers *ALB* and *AFP* in cells cultured in liver dECM-based scaffolds than those in other two groups (Fig. 2C). Collectively, these results demonstrate that the addition of liver dECM and collagen into the GelMA scaffolds better supported the viability of HepG2 cells compared to GelMA scaffolds alone, and that liver dECM-based scaffolds supported the highest level of expression of proliferation and metabolic markers overall.

3.3. Tuning the mechanical properties of 3D printed dECM-based scaffolds with negligible impacts on molecular diffusion

The improved viability and gene expression of HepG2 cells in the printed liver dECM-based scaffolds encouraged us to further explore the possibility of creating scaffolds with well-defined mechanical properties. We first investigated the relationship between printing conditions and scaffold mechanical property using our rapid 3D bioprinter. By varying the exposure time regionally, mechanical properties can be easily changed within the same construct (Fig. 3A). Similarly, scaffolds of uniform mechanical property can be printed using the corresponding exposure time (Fig. 3B). Mechanical testing measurements of the liver dECM-based constructs demonstrated a positive linear relationship between stiffness and exposure time as shown in Fig. 3C. In particular, three different exposure times of 10 s, 20 s, and 40 s were chosen to produce scaffolds with stiffness values of approximately 0.5 kPa, 5 kPa and 15 kPa, which each corresponds to the softer than healthy range (soft), healthy liver range (medium), and cirrhotic range (stiff), respectively [27]. Using these printing conditions, both acellular and cell-embedded scaffolds were fabricated and stiffness measurements were performed to determine the stability of the scaffolds across the 7-day culture period (Fig. 3B). In this case, the changes in stiffness over 7 days were not significant for all conditions in scaffolds with and without cells (Fig. 3D and E). Furthermore, diffusion profiles of fluorescent dextran molecules (4.4 kDa and 60–85 kDa respectively) into the printed constructs were compared between the soft, medium and stiff scaffolds over time (Figure S3, Supporting Information). No significant differences were observed in the amount of diffusion into each of the scaffolds at each time point (Fig. 3F and G). This indicated that increasing stiffness posed no significant impact on the diffusion of molecules with sizes larger than most growth factors. Overall, these results demonstrate

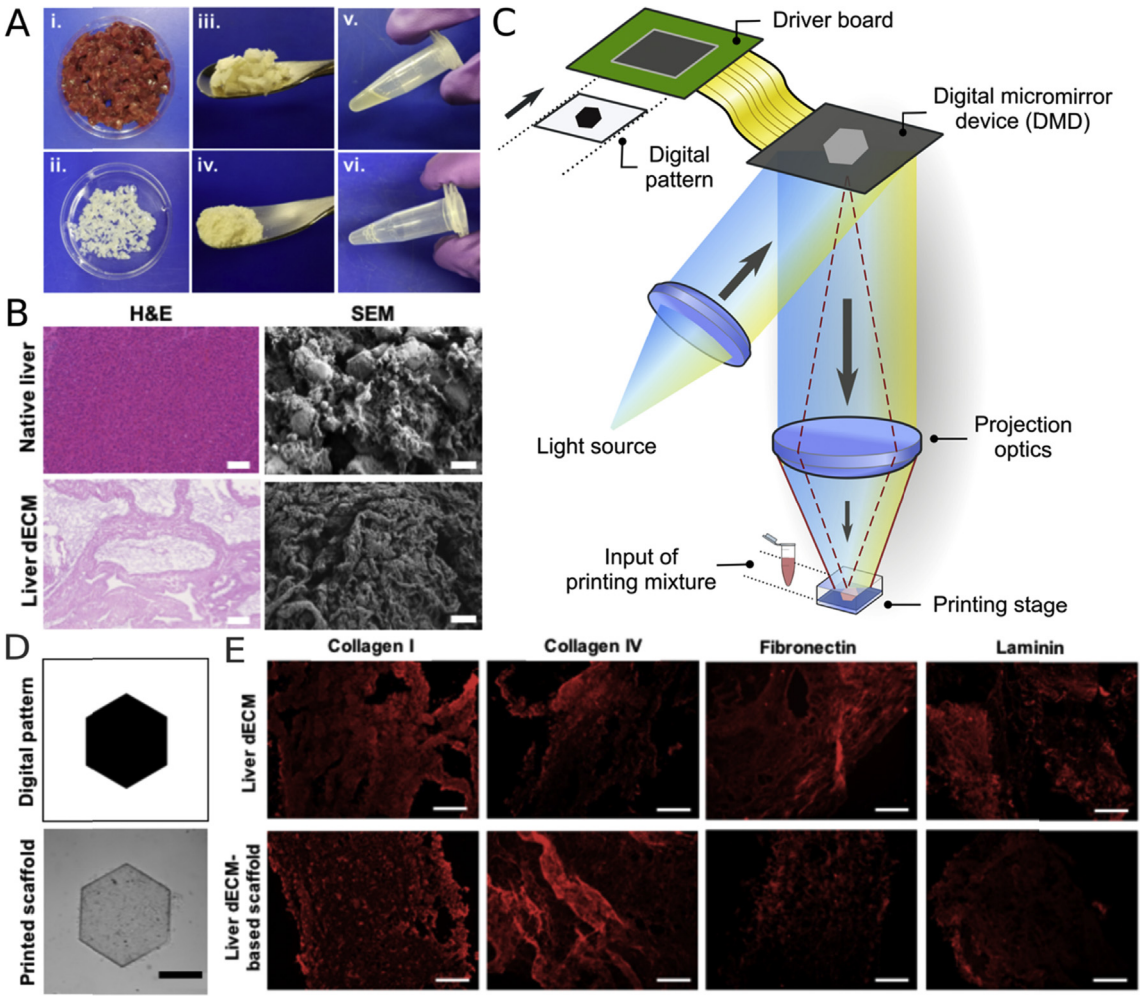

Fig. 1. 3D bioprinting of photocrosslinkable liver dECM-based hydrogel with key liver ECM components. (A) Decellularization of porcine liver and processing into a printable solution: i) fresh liver tissue, ii) liver dECM, iii) lyophilized liver dECM, iv) cryomilled liver dECM, v) pepsin solubilized liver dECM, vi) liver dECM-GelMA prepolymer solution to print liver dECM-based scaffolds. (B) Representative H&E stains and SEM images of the native liver and liver dECM showing full decellularization via removal of cells (scale bar = 100 μm) and preservation of intact collagen fibrils and ultrastructure (scale bar = 10 μm). (C) Schematic diagram showing the bioprinting of the dECM-based hexagonal scaffolds. (D) Digital pattern designed for bioprinting and the bright field image showing printed scaffolds using the pattern (scale bar = 500 μm). (E) Fluorescence images showing positive staining of collagen I, collagen IV, fibronectin, and laminin in pure liver dECM material and dECM-based scaffolds (scale bar = 200 μm).

that the rapid 3D bioprinting of liver dECM-based scaffolds provided a robust and stable mechanical environment for HepG2 cells over the entire culture period.

3.4. HCC demonstrated reduced proliferation and increased invasion potential in cirrhotic dECM scaffolds

To better understand how varying liver dECM-based matrix stiffness affects liver cancer cell growth and invasion potential, we characterized the viability, spheroid formation, and gene expression of encapsulated HepG2 cells. First, Live/Dead™ staining was performed on all three stiffness groups one day following printing (Fig. 4A). Quantification of live cell number showed greater than 80% viability in all groups with no significant difference between samples printed using different exposure times and with pre-printing cell suspension, which verified that the fabrication conditions did not negatively impact initial cell viability (Fig. 4B). Next, the cell viability and growth of HepG2 cells in the bioprinted liver dECM-based scaffolds of different stiffness were then monitored over 7 days (Fig. 4A). For scaffolds with soft and medium stiffness, cellular aggregation and spheroid formation was observed 3 days post printing with increasing spheroid size during the entire culture period. In contrast, only a few small aggregates were formed by HepG2 cells cultured in the stiff scaffolds. Measurements of the spheroid size for each stiffness group confirmed that a significantly higher growth of HepG2 cells was observed when cultured in the soft and medium scaffolds compared to minimal growth in the stiff dECM-based scaffolds (Fig. 4C).

To further confirm these observations, the expression of proliferation, apoptosis markers, and common liver-specific markers were investigated on day 7 of culture. No significant differences in expression for all markers was observed between cells cultured in soft and medium scaffolds. However, a significantly lower expression in the *MKI67, ALB*, and *AFP* was observed in HepG2 cells cultured in the stiff scaffolds along with a higher expression of the apoptosis marker *CASP8* (Fig. 4D). These results demonstrated that HepG2 cells exhibited a lower viability and slower growth when cultured in the stiff dECM-based scaffolds, and showed that a cirrhotic matrix stiffness significantly downregulated the expression of the liver-specific markers *ALB* and *AFP*.

Following the investigation of cancer cell growth, the impact of dECM-based scaffold stiffness on the migration and invasion potential of encapsulated HepG2 cells was assessed. The expression of insulin-like growth factor 2 (*IGF2*), which encodes for the angiogenesis factor that could accelerate tumor progression [28], was significantly higher in

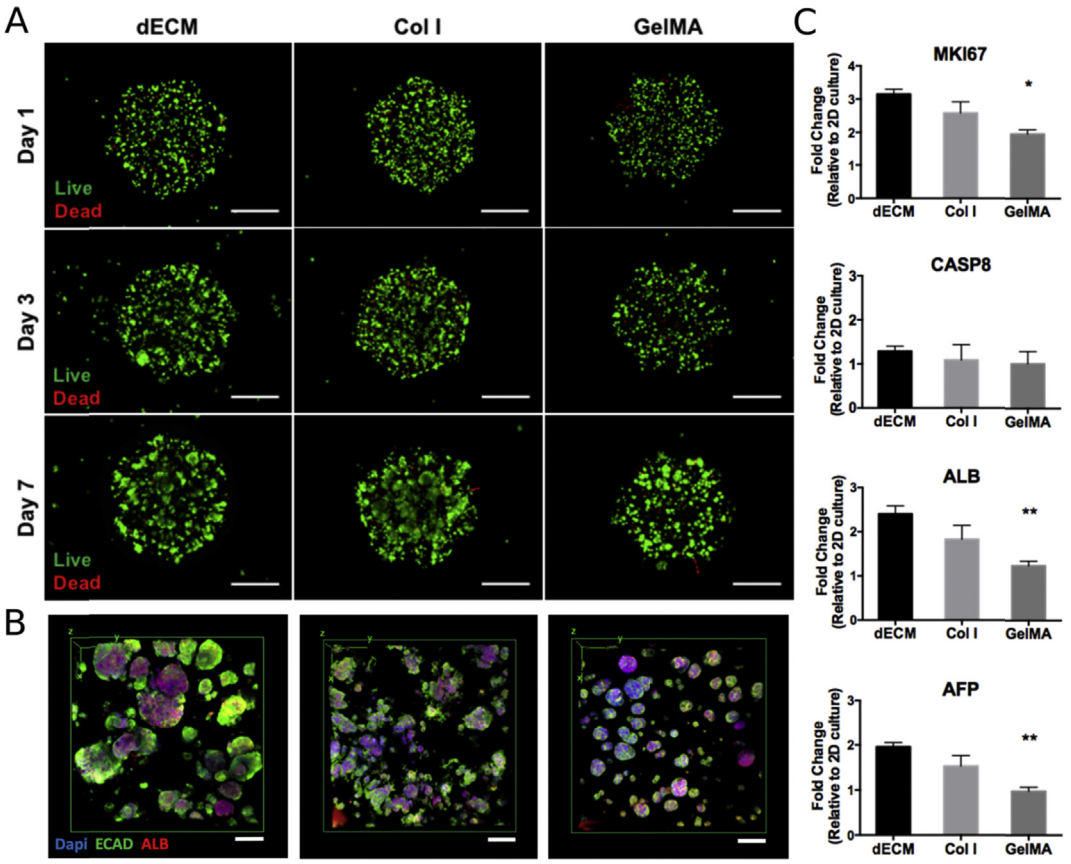

Fig. 2. Characterization of HepG2 cells cultured in dECM-based, collagen I-based, and GelMA constructs. (A) Fluorescence images showing Live/Dead™ stain of HepG2 cells cultured in dECM-based (dECM), collagen I-based (Col I), and GelMA constructs over 7 days (scale bar = 500 μm). (B) Fluorescence images showing staining of E-cadherin (ECAD) and albumin (ALB) in HepG2 cells cultured in dECM-based, collagen I-based, and GelMA constructs on day 7 (scale bar = 100 μm). (C) Gene expression analysis of MKI67, CASP8, ALB, and AFP of HepG2 cells cultured in dECM-based, collagen I-based and GelMA constructs on day 7. Error bars represent standard error of the mean, and n = 3 for all data points. *P ≤ 0.05, **P ≤ 0.01.

HepG2 cells cultured in the stiff scaffolds as compared to the soft and medium scaffolds after 7 days (Fig. 4E). Additionally, the expression of major matrix metalloproteinases (MMPs) *MMP2* and *MMP9* involved in HCC invasion were also upregulated in the stiff scaffolds as compared to the soft and medium conditions. Furthermore, a significantly higher expression of Twist-related protein 1 (*TWIST1*), which is correlated with HCC metastasis through the induction of epithelial-to-mesenchymal transition (EMT) [29], was observed in HepG2 cells cultured in the stiff and medium scaffolds (Fig. 4E). Together, these results demonstrated that a stiffer dECM-based scaffold induced an upregulation of genes encoded for ECM degradation enzymes and key transcriptional factors involved in EMT, which suggest a higher migration and invasion potential in these liver cancer cells.

3.5. Patterning dECM with regionally varied stiffness to visualize HCC stromal invasion

Encouraged by the results from the gene expression profile, we developed a 3D bioprinted liver cancer tissue platform to aid in visualizing the potential migration and invasion of HepG2 cells into surrounding tissues when cultured under various stiffness. The biomimetic design consists of three hexagonal lobules each possessing different stiffness that correspond to the soft, medium, and stiff scaffolds established prior. Each hexagonal unit is interconnected with a collagen I-based scaffold to represent the fibrous septa-like structure found in the fibrotic liver architecture (Fig. 5A). To monitor cell invasion from each hexagonal lobule into the surrounding collagenous septa, HepG2 cells in each region were stained using fluorescent CellTracker™ dye (i.e. red = soft, green = medium, yellow = stiff).

A total of four digital patterns were designed to print the final 3D liver cancer tissue platform (Figure S4, Supporting Information) in which three hexagonal patterns were used to print regions of three different stiffness and the last pattern for mimicking the inter-lobule fibrous septa. To minimize the possible effects of stiffness of the surrounding septa on HepG2 cell invasion, the collagen I-based septa regions were printed at similar mechanical properties as the healthy medium stiffness dECM-based hexagon (Figure S5, Supporting Information). Here, acellular constructs were first printed to test the feasibility of this printing approach followed by the printing of cell-embedded constructs (Fig. 5B).

Fluorescence and bright field images of the liver cancer tissue platform were evaluated over 7 days. A minimal amount of outgrowth from each of the hexagonal regions was observed across all conditions following the first day of culture. After 3 and 7 days of culture, an increased number of HepG2 cells was observed in the collagen septa region from the stiff scaffold, whereas fewer cells were observed crossing the septa-lobule boundary from the soft and medium conditions (Fig. 5C). To quantify the area of HepG2 cell outgrowth, all three hexagonal regions in the fluorescence images were blacked out and the cells present in the collagen septa region was quantified (Figure S6, Supporting Information). In this case, there was a significantly higher area of cellular outgrowth from the stiff matrix than from the other two conditions at 3 and 7 days (Fig. 5D). Taken together, this bioprinted liver cancer tissue platform could be used to visualize and quantify the invasion of HCC cells into the surrounding stromal regions. In this case, HepG2 cells cultured in a cirrhotic mechanical environment showed the

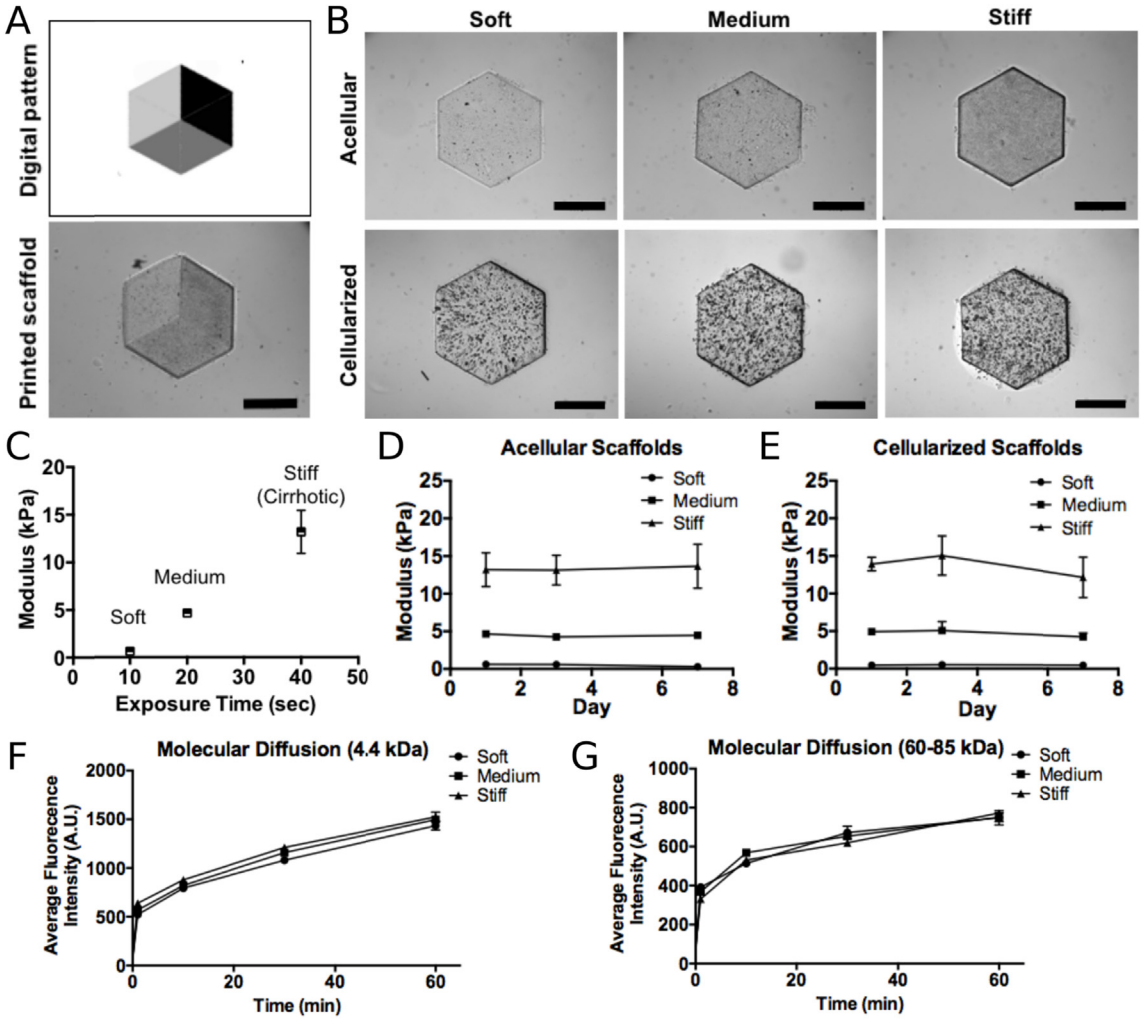

Fig. 3. 3D bioprinted liver dECM-based scaffolds with tunable stiffness. (A) Digital pattern (top) with greyscale used to control the exposure time in which the darker color corresponds to longer exposure time, and the bright field image (bottom) showing printed scaffolds using the pattern in which darker grey scale regions represent increased stiffness (scale bar = 500 μm). (B) Bright field images showing acellular and cellularized dECM-based scaffolds with three stiffness values (scale bar = 500 μm). (C) Plot showing the relationship between scaffold compressive modulus and printing exposure time one day after printing. n = 3 for all data points. (D) Quantitative plot showing the compressive moduli of acellular scaffolds over 7 days. n = 3 for all data points. (E) Quantitative plot showing the compressive moduli of cell-embedded scaffolds over 7 days. n = 5 for all data points. (F) Quantitative plot showing the average fluorescence intensity of dextran molecules (4.4 kDa) diffused into 3D printed dECM-based scaffolds. n = 4 for all data points. (G) Quantitative plot showing the average fluorescence intensity of dextran molecules (60–85 kDa) diffused into 3D printed dECM-based scaffolds. n = 4 for all data points. All error bars represent standard error of the mean.

highest degree of invasion into the adjacent septa regions. These observations were consistent with their high migration and invasion potential as observed at the genetic level for the stiff scaffolds.

4. Discussion

In recent studies examining liver cancer cell behavior in a cirrhotic mechanical environment, traditional 2D plating approaches have been met with limitations in predicting cellular responses that normally occur in a 3D *in vivo* milieu [7,8]. Furthermore, current 3D models with tunable stiffness mostly utilize simple biomaterials such as alginate and gelatin, which poorly recapitulate the complexity of the native liver microenvironment [10,11]. Cancer cell attachment and proliferation has also been demonstrated to vary depending on the type of biomaterial used [30]. Thus, naturally-derived dECM materials that better represent the liver ECM composition serve as an attractive candidate for engineering tissue models for liver cancer studies. In addition, past platforms studying liver cancer cell invasion and metastasis adopt simplistic designs that lack a biomimetic structure or well-defined mechanical properties, and have less physiologically relevant tissue properties necessary for elucidating liver cancer cell migration and invasion behavior [31]. To address these limitations, the goal of this study was to develop photocrosslinkable liver dECM and a rapid light-based 3D bioprinting process to pattern liver dECM with clinically relevant mechanical properties to serve as a biomimetic platform for HCC progression study.

Liver dECM biomaterials have been used in *in vitro* liver cell culture with increasing popularity due to its capability to provide a complex tissue-specific ECM microenvironment [17–19]. During the preparation of our dECM material, the preservation of liver microarchitecture and ultrastructure was shown in addition to the successful removal of cellular content. ECM proteins including GAG, collagen I, collagen IV, fibronectin, and laminin were also present in the dECM-based scaffolds demonstrating the successful preservation of key ECM components necessary for supporting cell culture. Future application of human-originated liver dECM materials is considered of greater benefits to the support of human liver cell culture. Furthermore, the development of a photocrosslinkable liver dECM-based hydrogel biomaterial enabled the use of liver dECM for DLP-based rapid 3D bioprinting, which has not been previously reported. Such application allows researchers to readily

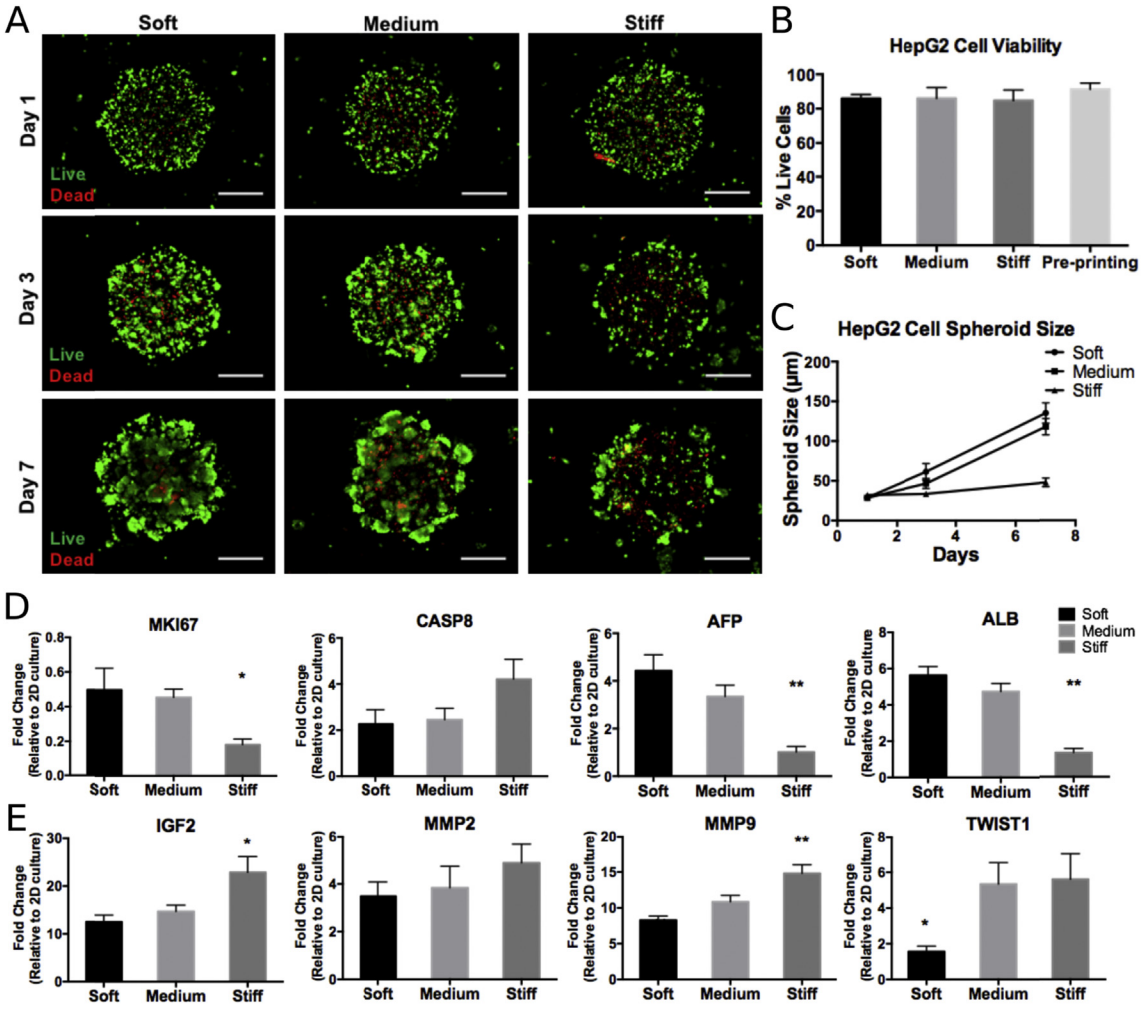

Fig. 4. Characterization of HCC growth and invasion potential in dECM-based scaffolds with varied stiffness. (A) Fluorescence images showing Live/Dead™ stain of HepG2 cells cultured in soft, medium, and stiff scaffolds over 7 days (scale bar = 500 μm). (B) Quantification of viable cell percentage in scaffolds of varied stiffness before and following cell encapsulation. n = 4–5. (C) Quantitative plot showing changes in HCC spheroid size over time under soft, medium, and stiff conditions. n = 3 for all data points. (D) Gene expression of MKI67, CASP8, ALB, and AFP of HepG2 cells cultured in soft, medium, and stiff conditions of dECM-based scaffolds on day 7. n = 4 for all data points. (E) Gene expression of IGF2, MMP2, MPP9, and TWIST1 in HepG2 cells cultured in scaffolds of varied stiffness. n = 4 for all data points. *P ≤ 0.05, **P ≤ 0.01. All error bars represent standard error of the mean.

print dECM-based hydrogel constructs with pre-determined shape and mechanical properties at high resolution within seconds.

The printed liver dECM-based scaffolds supported the culture of encapsulated HepG2 cells over 7 days *in vitro* as well as the expression of key liver genes and proteins. In particular, a similar number of viable cells in the dECM-based and collagen I-based hydrogels demonstrated that our liver dECM material was comparable to traditionally used collagen I for HepG2 cell culture. Fluorescent images confirmed the presence of liver albumin and epithelial marker in the HepG2 cell encapsulated dECM-based, collagen I-based, and GelMA scaffolds. These positive results are consistent with literature findings that liver dECM, GelMA, and collagen I support HepG2 cell and hepatocyte viability and morphology [19,22,32]. A further evaluation of gene expression revealed a better supportive role of the liver dECM-based scaffold on HepG2 cells than collagen I-based and GelMA scaffolds, as evident by the higher relative expression of *ALB, AFP, and MKI67*. This is consistent with the role of decellularized ECM scaffolds as a cell-instructive substrate to promote cell functionality and phenotype in a tissue-specific manner [33,34].

In this work, our rapid DLP-based 3D bioprinting technology enabled the flexible design of physiologically relevant geometries as well as precise control over hydrogel mechanical properties. Notably, this capability to create complex acellular and cell-embedded dECM-based hydrogel constructs has not yet been achieved by other 3D bioprinting platforms in liver tissue engineering [20,35]. By changing the light exposure time, changes in stiffness can be easily controlled without modifying the hydrogel components and thus eliminating effects contributed by different material concentrations or chemical composition on cell behavior. Furthermore, the similar diffusion profiles of dextran molecules into soft, medium and stiff constructs suggested that increased gel stiffness did not pose significant barrier to molecular diffusion to encapsulated cells.

Following the establishment of a stable 3D liver dECM-based hydrogel platform with well-defined mechanical properties, the response of HepG2 cells to varying degrees of stiffness was then evaluated. The high viability of HepG2 cells observed in all conditions one day after printing confirmed that the variation in 3D bioprinting exposure time did not affect initial cell viability. However, a decrease in HepG2 cell viability on day 3 and 7 of culture with considerably smaller spheroid size indicated that there was significant growth restriction on HepG2 cells when embedded in dECM-based scaffolds with a stiffness similar to cirrhotic liver. These findings are consistent with literature reports on reduced viability and growth in cancer cells cultured in stiff 3D hydrogels [9,36]. A further evaluation on the gene expression confirmed

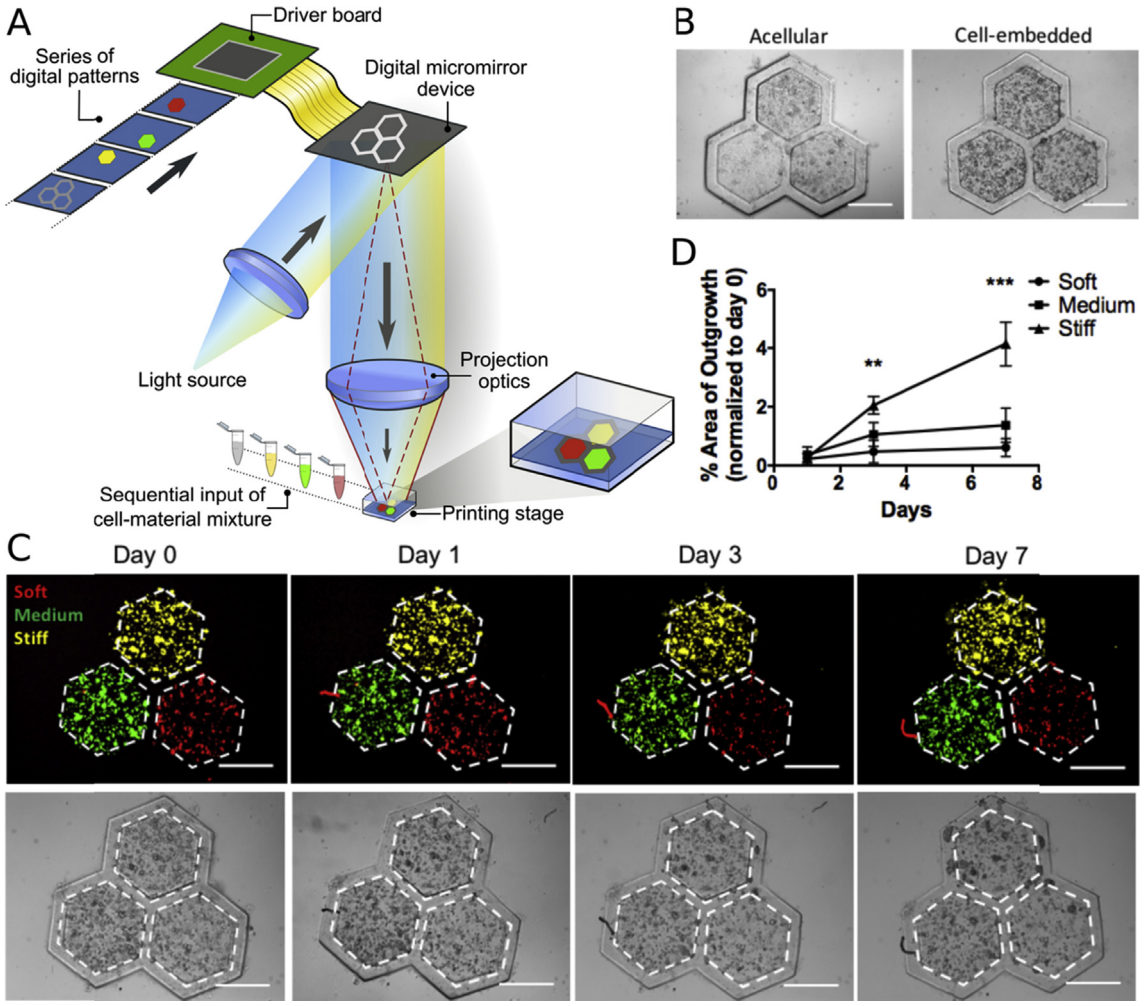

Fig. 5. 3D bioprinted liver cancer tissue platform with varied scaffold stiffness. (A) Schematic diagram showing the bioprinting setup of the dECM-based liver cancer tissue platform. (B) Bright field images showing printed scaffolds without and with cells (scale bar = 500 μm). (C) Merged fluorescence and paired bright field images showing the tracked HepG2 cell locations relative to their assigned hexagonal regions over 7 days. Red = soft, green = medium, yellow = stiff condition. (scale bar = 500 μm). (D) Quantitative plot showing the percent area of cell invasion originating from the three different scaffolds over time. Error bars represent standard error of the mean, and n = 5 for all data points. **P ≤ 0.01, ***P ≤ 0.001. (For interpretation of the references to color in this figure legend, the reader is referred to the Web version of this article.)

these results as attributed by the lower levels of the proliferation marker *MKI67*, *ALB*, and *AFP* expression coupled with higher levels of the apoptosis marker *CASP8*. Overall, a stiff scaffold similar to that of cirrhotic liver markedly reduced liver-specific gene expression and cell proliferation in HepG2 cells, and supports the hypothesis that a cirrhotic mechanical environment plays a significant role in liver function impairment in patients with cirrhosis and HCC [37].

In addition to the effects of stiffness on HepG2 cell growth, the impacts of the cirrhotic matrix on HepG2 cell migratory and invasive behavior is critical in better understanding the observed increase in liver cancer malignancy under cirrhotic conditions [2]. Significantly elevated expression of *IGF2* in HepG2 cells cultured in scaffolds with cirrhotic liver stiffness suggests that this disease-related mechanical environment could potentially accelerate tumor progression [28]. Both *MMP2* and *MMP9* encode for key enzymes involved in degradation of basement membrane proteins and are closely correlated to HCC tumor invasion, metastasis, and recurrence [38]. More specifically, the high expression of both *MMP2* and *MMP9* in the stiffest scaffold points to an increased potential for migration and invasion behavior of HCC cells due to the cirrhotic mechanical environment. In particular, significantly higher *MMP9* expression is strongly correlated to a more advanced tumor stage and higher HCC recurrence risk [39]. These findings may help partially explain the high mortality rate in patients with HCC since its development is strongly coupled with liver cirrhosis [1,2]. Furthermore, the higher expression of *TWIST1* in HepG2 cells cultured in both the medium and stiff scaffolds also indicated a higher possibility of EMT induction and HCC metastasis within a cirrhotic environment [29].

With the observed increase in migration and invasion potential of HepG2 cells induced by the cirrhotic matrix stiffness at the genetic level, the ability to visualize this behavior *in vitro* would be a valuable tool for monitoring cancer cell dynamics under diseased conditions. Common *in vitro* cancer migration and invasion platforms use traditional approaches such as scratch assays, transwell cell invasion assays, and spheroid encapsulation invasion assays [40,41]. While these studies contribute some information on the tendency of cancer cell migration, they are very limited in providing a biomimetic 3D environment to recapitulate the stromal invasion process where liver cancer cells demonstrate invasive growth into the portal tracts and fibrous septa. Here, the establishment of an engineered liver cancer tissue platform that incorporates the fibrous septa between liver nodules of varied stiffness served as a biomimetic platform to visualize the effect of cirrhotic matrix stiffness on the invasion of HepG2 cells into the fibrous septa regions. In particular, the ability to rapidly and precisely pattern different cells and biomaterials into their assigned locations using our

3D bioprinting platform enabled the fabrication of the complex native liver microarchitecture with micron scale resolution. By labelling the cells with different fluorescent CellTracker™ dyes corresponding to scaffolds of different stiffness, the encapsulated HepG2 cells could be easily and clearly tracked in a visual manner for invasion behavior. In this design, the collagen I-based septa region was chosen to have a stiffness matched to the dECM-based hexagon of medium stiffness to reduce any potential for spontaneous outgrowth of HepG2 cells from the dECM-based lobules into the collagen I-based septa regions due to abnormal mechanical properties. Furthermore, a minimal amount of invasion of HCC occurred when they were cultured in the medium stiffness condition, thus suggesting that the cells did not migrate towards the collagen I-based septa regions because of differences in biomaterial composition. Interestingly, a higher degree of invasion into the surrounding septa regions of HepG2 cells originating from the stiff hexagonal region demonstrated that HCC cells cultured in a cirrhotic matrix stiffness were more invasive as compared to those in healthy or softer matrices. Therefore, we conclude that the increased migratory and invasive behavior observed from this engineered liver cancer tissue platform is primarily due to the cirrhotic scaffold stiffness. These results have profound implications that high stiffness alone in a cirrhotic liver could play a significant role to potentiate cancer stromal invasion and future metastasis. Furthermore, liver tissue mechanical property, currently used as a fibrosis diagnostic marker and HCC risk prediction [27], could later be identified as a therapeutic target for reducing HCC invasion and metastasis in patients with advanced fibrotic and cirrhotic liver disease.

5. Conclusions

In this study, photocrosslinkable liver dECM with well-preserved key ECM components was developed and readily printed into liver lobule architectures using DLP-based rapid 3D bioprinting. The liver dECM-based scaffolds not only supported cell viability but also provided a stable physiologically relevant mechanical environment. When encapsulated in dECM scaffolds with cirrhotic stiffness, HepG2 cells demonstrated reduced growth along with an upregulation of invasion markers compared to healthy controls. Moreover, 3D bioprinting of liver dECM in hexagonal nodules of varied stiffness enabled visualization of stromal invasion behavior from the nodule with cirrhotic liver stiffness which were consistent with findings at the genetic level.

The successful combination of this DLP-based 3D bioprinting technology with liver dECM-based hydrogels highlights the progress of the field to a level where complex ECM materials can be utilized to create micro-patterned scaffolds with targeted physical properties for biological studies. Further optimization on the distribution of biomaterials and stiffness according to clinical data as well as incorporating patient cell sources such as primary HCC cells and other relevant non-parenchymal cells could open the door to establishing a more sophisticated liver fibrosis or cirrhosis disease model with potential to serve as early anticancer drug screening platforms. The 3D bioprinted dECM-based platform in this study enables the visualization of the invasive response of HCC cells in scaffolds with cirrhotic liver stiffness and demonstrates great potential as a platform technology for pathophysiological studies and drug screening in the future.

Author contributions

X.M., P.W. and S.C. conceived the study. C.Y., P.W., J.L. and A.K-M. prepared dECM and GelMA materials. X.M., C.Y. and P.W. carried out material characterization. X.M., W.X., X.W. and C.S.E.L. designed and performed the cell experiments and assays. X.M., C.Y., P.W., W.X. and X.W. analyzed the data. X.M., C.Y. and S.C. wrote the manuscript.

Conflicts of interest

The authors declare no competing financial interests.

Data availability

The raw/processed data required to reproduce these findings can be shared by the authors upon request.

Acknowledgements

We thank Shangting You, Dr. David Berry, Jacob Stupin, and Alexandria Hairabedian for their technical assistance. We would also like to thank the staff at Moores Cancer Center Histology Core for performing the H&E staining of the samples, as well as Patricia Pizarro at the Center for the Future of Surgery for providing the porcine liver tissues used in this study. This work was supported by National Institutes of Health (Grant # EB021857 and HD090662) and National Science Foundation (Grant # 1547005 and 1644967). The University of California, San Diego Neuroscience Microscopy Shared Facility was supported by Grant P30 (NS047101) from the National Institutes of Health. Scholarship funding for Dr. Claire Yu was provided by the Natural Sciences and Engineering Research Council (NSERC) Postdoctoral Fellowship Scholarship of Canada.

Appendix A. Supplementary data

Supplementary data to this article can be found online at https://doi.org/10.1016/j.biomaterials.2018.09.026.

References

[1] J. Ferlay, I. Soerjomataram, R. Dikshit, S. Eser, C. Mathers, M. Rebelo, D.M. Parkin, D. Forman, F. Bray, Cancer incidence and mortality worldwide: sources, methods and major patterns in GLOBOCAN, Int. J. Cancer. 136 (2012) 2015, https://doi.org/10.1002/ijc.29210 E359–E386.
[2] G. Fattovich, T. Stroffolini, I. Zagni, F. Donato, Hepatocellular carcinoma in cirrhosis: incidence and risk factors, Gastroenterology 127 (2004) S35–S50.
[3] D. Schuppan, N.H. Afdhal, Liver cirrhosis, Lancet 371 (2008) 838–851, https://doi.org/10.1016/S0140-6736(08)60383-9.
[4] R. Masuzaki, R. Tateishi, H. Yoshida, T. Sato, T. Ohki, T. Goto, H. Yoshida, S. Sato, Y. Sugioka, H. Ikeda, S. Shiina, T. Kawabe, M. Omata, Assessing liver tumor stiffness by transient elastography, Hepatol. Int. 1 (2007) 394–397, https://doi.org/10.1007/s12072-007-9012-7.
[5] W. Ling, Q. Lu, C. Lu, J. Quan, L. Ma, J. Li, D. He, J. Liu, J. Yang, T. Wen, H. Wu, H. Zhu, Y. Luo, Effects of vascularity and differentiation of hepatocellular carcinoma on tumor and liver stiffness: in vivo and in vitro studies, Ultrasound Med. Biol. 40 (2014) 739–746, https://doi.org/10.1016/j.ultrasmedbio.2013.08.011.
[6] F. Kondo, Histological features of early hepatocellular carcinomas and their developmental process: for daily practical clinical application, Hepatol. Int. 3 (2009) 283–293, https://doi.org/10.1007/s12072-008-9107-9.
[7] J. Schrader, T.T. Gordon-Walker, R.L. Aucott, M. van Deemter, A. Quaas, S. Walsh, D. Benten, S.J. Forbes, R.G. Wells, J.P. Iredale, Matrix stiffness modulates proliferation, chemotherapeutic response, and dormancy in hepatocellular carcinoma cells, Hepatology 53 (2011) 1192–1205, https://doi.org/10.1002/hep.24108.
[8] A.D. Doyle, K.M. Yamada, Mechanosensing via cell-matrix adhesions in 3D microenvironments, Exp. Cell Res. 343 (2016) 60–66, https://doi.org/10.1016/j.yexcr.2015.10.033.
[9] M.K. Aparnathi, J.S. Patel, P.D. Patel, Effect of gel porosity and stiffness on culture of HepG2 cells encapsulated in gelatin methacrylate hydrogels, Biosci. Biotech. Res. Commun. 9 (2016) 463–470.
[10] R. Zhang, M. Ma, G. Dong, R.-R. Yao, J.-H. Li, Q.-D. Zheng, Y.-Y. Dong, H. Ma, D.-M. Gao, J.-F. Cui, Z.-G. Ren, R.-X. Chen, Increased matrix stiffness promotes tumor progression of residual hepatocellular carcinoma after insufficient heat treatment, Canc. Sci. 108 (2017) 1778–1786, https://doi.org/10.1111/cas.13322.
[11] Y. You, Q. Zheng, Y. Dong, Y. Wang, L. Zhang, T. Xue, X. Xie, C. Hu, Z. Wang, R. Chen, Y. Wang, J. Cui, Z. Ren, Higher matrix stiffness upregulates osteopontin expression in hepatocellular carcinoma cells mediated by integrin β1/GSK3β/β-catenin signaling pathway, PLoS One 10 (2015), https://doi.org/10.1371/journal.pone.0134243 e0134243.
[12] C. Liu, Y. Liu, H. Xie, S. Zhao, X. Xu, L. Fan, X. Guo, T. Lu, G.-W. Sun, X. Ma, Role of three-dimensional matrix stiffness in regulating the chemoresistance of hepatocellular carcinoma cells, Biotechnol. Appl. Biochem. 62 (2015) 556–562, https://doi.org/10.1002/bab.1302.
[13] S. Pradhan, I. Hassani, J.M. Clary, E.A. Lipke, Polymeric biomaterials for in vitro cancer tissue engineering and drug testing applications, Tissue Eng. Part B. Rev. 22

(2016) 470–484, https://doi.org/10.1089/ten.TEB.2015.0567.
[14] B.E. Uygun, A. Soto-Gutierrez, H. Yagi, M.-L. Izamis, M.A. Guzzardi, C. Shulman, J. Milwid, N. Kobayashi, A. Tilles, F. Berthiaume, M. Hertl, Y. Nahmias, M.L. Yarmush, K. Uygun, Organ reengineering through development of a transplantable recellularized liver graft using decellularized liver matrix, Nat. Med. 16 (2010) 814–820, https://doi.org/10.1038/nm.2170.
[15] G. Mazza, K. Rombouts, A. Rennie Hall, L. Urbani, T. Vinh Luong, W. Al-Akkad, L. Longato, D. Brown, P. Maghsoudlou, A.P. Dhillon, B. Fuller, B. Davidson, K. Moore, D. Dhar, P. De Coppi, M. Malago, M. Pinzani, Decellularized human liver as a natural 3D-scaffold for liver bioengineering and transplantation, Sci. Rep. 5 (2015) 13079, https://doi.org/10.1038/srep13079.
[16] P.M. Baptista, M.M. Siddiqui, G. Lozier, S.R. Rodriguez, A. Atala, S. Soker, The use of whole organ decellularization for the generation of a vascularized liver organoid, Hepatology 53 (2011) 604–617, https://doi.org/10.1002/hep.24067.
[17] K.-M. Park, K.H. Hussein, S.-H. Hong, C. Ahn, S.-R. Yang, S.-M. Park, O.-K. Kweon, B.-M. Kim, H.-M. Woo, Decellularized liver extracellular matrix as promising tools for transplantable bioengineered liver promotes hepatic lineage commitments of induced pluripotent stem cells, Tissue Eng. Part A 22 (2016) 449–460, https://doi.org/10.1089/ten.tea.2015.0313.
[18] Y. Wang, C.-B. Cui, M. Yamauchi, P. Miguez, M. Roach, R. Malavarca, M.J. Costello, V. Cardinale, E. Wauthier, C. Barbier, D.A. Gerber, D. Alvaro, L.M. Reid, Lineage restriction of human hepatic stem cells to mature fates is made efficient by tissue-specific biomatrix scaffolds, Hepatology 53 (2011) 293–305, https://doi.org/10.1002/hep.24012.
[19] Y. Cheng, Y. Wang, Y.Z. Kang, P.Y. Hu, Y. Gao, M.X. Pan, In vitro culture of tumour-derived hepatocytes in decellularised whole-liver biological scaffolds, Digestion 87 (2013) 189–195, https://doi.org/10.1159/000349949.
[20] H. Lee, W. Han, H. Kim, D.-H. Ha, J. Jang, B.S. Kim, D.-W. Cho, Development of liver decellularized extracellular matrix bioink for three-dimensional cell printing-based liver tissue engineering, Biomacromolecules 18 (2017) 1229–1237, https://doi.org/10.1021/acs.biomac.6b01908.
[21] J.S. Lee, J. Shin, H.M. Park, Y.G. Kim, B.G. Kim, J.W. Oh, S.W. Cho, Liver extracellular matrix providing dual functions of two-dimensional substrate coating and three-dimensional injectable hydrogel platform for liver tissue engineering, Biomacromolecules 15 (2014) 206–218, https://doi.org/10.1021/bm4015039.
[22] X. Ma, X. Qu, W. Zhu, Y.-S. Li, S. Yuan, H. Zhang, J. Liu, P. Wang, C.S.E. Lai, F. Zanella, G.-S. Feng, F. Sheikh, S. Chien, S. Chen, Deterministically patterned biomimetic human iPSC-derived hepatic model via rapid 3D bioprinting, Proc. Natl. Acad. Sci. 113 (2016) 2206–2211, https://doi.org/10.1073/pnas.1524510113.
[23] W. Zhu, X. Qu, J. Zhu, X. Ma, S. Patel, J. Liu, P. Wang, C.S.E. Lai, M. Gou, Y. Xu, K. Zhang, S. Chen, Direct 3D bioprinting of prevascularized tissue constructs with complex microarchitecture, Biomaterials 124 (2017) 106–115, https://doi.org/10.1016/j.biomaterials.2017.01.042.
[24] M. Gou, X. Qu, W. Zhu, M. Xiang, J. Yang, K. Zhang, Y. Wei, S. Chen, Bio-inspired detoxification using 3D-printed hydrogel nanocomposites, Nat. Commun. 5 (2014) 3774, https://doi.org/10.1038/ncomms4774.
[25] P.M. Crapo, T.W. Gilbert, S.F. Badylak, An overview of tissue and whole organ decellularization processes, Biomaterials 32 (2011) 3233–3243, https://doi.org/10.1016/j.biomaterials.2011.01.057.
[26] Y.-J. Wang, H.-L. Liu, H.-T. Guo, H.-W. Wen, J. Liu, Primary hepatocyte culture in collagen gel mixture and collagen sandwich, World J. Gastroenterol. 10 (2004) 699–702, https://doi.org/10.3748/WJG.V10.I5.699.
[27] S. Mueller, L. Sandrin, Liver stiffness: a novel parameter for the diagnosis of liver disease, Hepat. Med. 2 (2010) 49–67.
[28] H. Thomas, Liver cancer: IGF2 — an epigenetic oncodriver in HCC, Nat. Rev. Gastroenterol. Hepatol. 13 (2016), https://doi.org/10.1038/nrgastro.2016.162 625–625.
[29] T.K. Lee, R.T.P. Poon, A.P. Yuen, M.T. Ling, W.K. Kwok, X.H. Wang, Y.C. Wong, X. Guan, K. Man, K.L. Chau, S.T. Fan, Twist overexpression correlates with hepatocellular carcinoma metastasis through induction of epithelial-mesenchymal transition, Clin. Cancer Res. 12 (2006) 5369–5376, https://doi.org/10.1158/1078-0432.CCR-05-2722.
[30] M.R. Carvalho, D. Lima, R.L. Reis, V.M. Correlo, J.M. Oliveira, Evaluating biomaterial-and microfluidic-based 3D tumor models, Trends Biotechnol. 33 (2015) 667–678, https://doi.org/10.1016/j.tibtech.2015.09.009.
[31] Q.F. Ye, S.X. Cai, X.Z. Dai, X.Q. Yan, M.S. Zou, Z. Xu, Effects of matrix viscoelasticity on HepG2 cell metastasis in a microfluidic device, J. Med. Biol. Eng. 33 (2013) 163–170, https://doi.org/10.5405/jmbe.1094.
[32] J.V. Castell, M.J. Gomez-Lechon, Hepatocyte transplantation, Methods Mol. Biol. 481 (2009) 35–46, https://doi.org/10.1007/978-1-59745-201-4_4.
[33] K.P. Robb, A. Shridhar, L.E. Flynn, Decellularized matrices as cell-instructive scaffolds to guide tissue-specific regeneration, ACS Biomater. Sci. Eng. ASAP (2017), https://doi.org/10.1021/acsbiomaterials.7b00619.
[34] Y. Zhang, Y. He, S. Bharadwaj, N. Hammam, K. Carnagey, R. Myers, A. Atala, M. Van Dyke, Tissue-specific extracellular matrix coatings for the promotion of cell proliferation and maintenance of cell phenotype, Biomaterials 30 (2009) 4021–4028, https://doi.org/10.1016/j.biomaterials.2009.04.005.
[35] F. Pati, J. Jang, D.-H. Ha, S. Won Kim, J.-W. Rhie, J.-H. Shim, D.-H. Kim, D.-W. Cho, Printing three-dimensional tissue analogues with decellularized extracellular matrix bioink, Nat. Commun. 5 (2014) 1–11, https://doi.org/10.1038/ncomms4935.
[36] M. Cavo, M. Fato, L. Peñuela, F. Beltrame, R. Raiteri, S. Scaglione, Microenvironment complexity and matrix stiffness regulate breast cancer cell activity in a 3D in vitro model, Sci. Rep. 6 (2016) 35367, https://doi.org/10.1038/srep35367.
[37] M. Pinter, M. Trauner, M. Peck-Radosavljevic, W. Sieghart, Cancer and liver cirrhosis: implications on prognosis and management, ESMO Open 1 (2016), https://doi.org/10.1136/esmoopen-2016-000042 e000042.
[38] Y. Itoh, Membrane-type matrix metalloproteinases: their functions and regulations, Matrix Biol. 44–46 (2015) 207–223, https://doi.org/10.1016/j.matbio.2015.03.004.
[39] J.P. Kuyvenhoven, B. Van Hoek, E. Blom, W. Van Duijn, R. Hanemaaijer, J.H. Verheijen, C.B.H.W. Lamers, H.W. Verspaget, Assessment of the clinical significance of serum matrix metalloproteinases MMP-2 and MMP-9 in patients with various chronic liver diseases and hepatocellular carcinoma, Thromb. Haemost. 89 (2003) 718–725, https://doi.org/10.1267/THRO03040718.
[40] E. Wiercinska, H.P.H. Naber, E. Pardali, G. van der Pluijm, H. van Dam, P. ten Dijke, The TGF-β/Smad pathway induces breast cancer cell invasion through the up-regulation of matrix metalloproteinase 2 and 9 in a spheroid invasion model system, Breast Cancer Res. Treat. 128 (2011) 657–666, https://doi.org/10.1007/s10549-010-1147-x.
[41] C.R. Justus, N. Leffler, M. Ruiz-Echevarria, L. V Yang, In vitro cell migration and invasion assays, J. Vis. Exp. (2014) 1–8, https://doi.org/10.3791/51046.